Development of a Phoswich Detector for Radioxenon Field Measurements

W. Hennig, *Member, IEEE*, S. J. Asztalos, W. K. Warburton, A. Fallu-Labruyere, *Member, IEEE*, A. Samie, and P. Mekarski

***Abstract*—The Comprehensive Nuclear-Test-Ban Treaty Organization deploys a variety of radioxenon detection systems as part of its International Monitoring System to detect nuclear explosions. To achieve the high sensitivity required, the systems extract xenon from several cubic meters of air and look for characteristic radioactive emissions, using either high resolution high purity germanium gamma detectors or multiple scintillators for high efficiency beta/gamma coincidence detection. The high sensitivity comes at the expense of heavy lead shielding, and for the latter, calibration and gain matching of multiple photomultiplier tubes as well as a memory effect of the plastic scintillator used for beta detection which absorbs Xe. Existing systems are also stationary by design, though in some applications, for example on-site inspections, a portable detector is required. In this work, we therefore redesigned a previously developed phoswich detector to reduce size, weight, cost, complexity and memory effect with only minor impact on the sensitivity. The phoswich design requires only a single photomultiplier tube with beta/gamma coincidences being detected by digital pulse shape analysis. Additional gain stabilization addresses varying environmental field conditions, such as temperature changes. Three phoswich geometries were modeled through Monte Carlo simulations, the most promising was built and tested. In this paper we describe each of the initial designs, their simulated performances and the factors that lead us to the chosen design. Preliminary results from testing of the prototype detector are presented and compared with simulation.**

***Index Terms*—Nuclear explosion monitoring, phoswich scintillation counter, radioxenon detection.**

I. Introduction

THE Comprehensive Nuclear-Test-Ban Treaty (CTBT) establishes the development of the International Monitoring System (IMS) to detect nuclear explosions in violation of the treaty. Even though the treaty is not yet in force and the IMS not fully completed, it has demonstrated its relevance to international security by the detection of radioxenon from North Korea's nuclear tests and from the Fukushima reactor accident [1]. The IMS radioxenon detector systems include the SAUNA [2], ARIX, and SPALAX [3] system; several research laboratories also use the ARSA detector [4]. Radioxenon isotopes of interest are ^{133}Xe, ^{131m}Xe, ^{133m}Xe, and ^{135}Xe, emitting 30, 80, and 250 keV photons in coincidence with conversion electrons (CE) and/or beta particles in the range from 45 to 905 keV (see Table I). The SAUNA and ARSA systems detect beta/gamma coincidences with arrangements of multiple scintillators, while the SPALAX detects photons with high resolution with a HPGe gamma-ray detector. These established radioxenon detectors reach minimum detectable concentrations (MDC) of less than 1 mBq/m^3 for ^{133}Xe, as specified by the IMS, but possess a number of design drawbacks: the SPALAX system requires cryogenic cooling, and the multiple detectors of the SAUNA and ARSA systems make them not only cumbersome to calibrate but also complex and bulky. The plastic scintillator used for beta detection also absorbs Xe, which leads to a "memory effect" where previous samples contribute to the background in subsequent measurements. The effect is about 3-8%, varying with detector geometry. In addition, all detectors are designed to be installed in permanent IMS stations or laboratories where weight and volume are not an issue, while in some applications a portable detector is required, for example CTBTO on-site inspections (OSI).

TABLE I
KEY DECAY ENERGIES FROM RADIOXENON ISOTOPES USED IN NUCLEAR EXPLOSION MONITORING [5]

isotope	Half life	Energy (keV)	Intensity (%)	Type
^{131m}Xe	11.9 d	29-34	54.0	K X-rays
		129	60.7	CE
^{133m}Xe	2.19 d	29-34	56.3	K X-rays
		199	63.1	CE
^{133}Xe	5.245 d	31-36	48.9	K X-rays
		45	54.1	CE
		346	100	Beta (endpoint)
^{135}Xe	9.1 h	31-36	5.2	K X-rays
		214	5.7	CE
		250	90	gamma
		910	100	Beta (endpoint)

To reduce the complexity of these detectors, several new detectors have been developed in recent years. For example, efforts were made to simplify and redesign a beta/gamma well detector with CsI and BC-404 scintillators [6], and to modify the SAUNA detector for a portable version [7]. Al_2O_3 coating of the BC-404 was studied to reduce the memory effect [8], [9]. A more sophisticated concept, first described in [10] for radioxenon detectors, is the use of optically coupled scintillators in a phoswich detector read out with a single photomultiplier

Manuscript received March 07, 2014; revised July 07, 2014; accepted July 19, 2014. Date of publication September 05, 2014; date of current version October 09, 2014. This work was supported by the U.S. Department of Energy under Award DE-NA0001522.

W. Hennig, S. J. Asztalos, and W. K. Warburton are with XIA LLC, Hayward, CA 94544-7831 USA (e-mail: whennig@xia.com).

A. Fallu-Labruyere and A. Samie are with Mirion Technologies (MGPI) SA, F-13113 Lamanon, France.

P. Mekarski is with the Radiation Protection Bureau of Health Canada, Ottawa, ON K1A 1C1, Canada.

Digital Object Identifier 10.1109/TNS.2014.2343158

tube (PMT) and application of digital pulse shape analysis to detect coincidences. Other examples of radioxenon phoswich detectors are the PhosWatch [11], a CsI/BC-404 well detector, and a planar triple layer detector with BC-400, NaI and $\mathrm{CaF_2}$ [12]. More recent work explores the use of silicon detectors, for example in multi-channel silicon-only detectors for beta/X-ray coincidences [13] or as alternative beta detectors in a beta/gamma detector [14], [15], [16].

In the work described here, we redesigned the PhosWatch (PW) detector to reduce size, weight, cost, complexity, and memory effect with only minor impact on the sensitivity. Rugged packaging and built-in gain stabilization address the requirements for portable applications. In a first stage, three conceptual designs of this "Portable PhosWatch" (PPW) were modeled through Monte Carlo simulations to determine the detection efficiency, the light collection and the resulting energy resolution, the impact of memory effect mitigations, and the influence of background. In a second stage, the most promising design was manufactured, assembled in the rugged portable packaging, and tested with a variety of test sources, including $^{222}\mathrm{Rn}$ and $^{133}\mathrm{Xe}$.

II. Detector Modeling

A. Detector Geometries and Efficiencies

To evaluate conceptual design performance, Monte Carlo simulations were carried out on three possible PPW geometries and compared with the PhosWatch detector. Geant4 [17], [18] code developed previously [19] to model the PhosWatch detector was adapted and used to determine the (relative) energy resolution and detection efficiencies for the new geometries. The modifications to the original code were primarily limited to the CsI and BC404 topologies. No modifications were needed to the standard physics lists for these simulations.

The three PPW geometries (shown in Fig. 1 together with the original PhosWatch geometry) were chosen based on the following considerations: First, to match standard PMT sizes, the CsI crystal should be a cylinder of 50.8 mm or 76.2 mm diameter. Second, half of a 50.8 mm diameter CsI crystal has sufficient stopping power for 30 and 80 keV photons and 1 mm BC-404 has sufficient stopping power for electrons up to 345 keV. Thus only the 250 keV $\mathrm{gamma} + 905$ keV beta coincidences from $^{135}\mathrm{Xe}$ are detected with significantly higher efficiency in a larger crystal such the PhosWatch (76.2 mm) or SAUNA (101.6 mm) and with a thicker plastic scintillator. While this isotope provides valuable information on the radioxenon origin, it is rarely encountered in IMS stations and very unlikely in an OSI application, having mostly decayed by the time the OSI team arrives. A smaller detector also requires less shielding. Third, though the spherical design of the PhosWatch Xe cell provides close to 4π coverage, it is difficult to manufacture, especially if beta scintillators other than BC-404 are to be used. Fourth, scintillator interfaces parallel to the PMT window are to be avoided because of poor light collection [20]. Overall, geometries of interest are therefore narrowed to 50.8 mm CsI crystals with simple interfaces perpendicular to the PMT window, which implies a Xe cell in the shape of a cylinder or prism. The first geometry (cylinder) is thus a BC-404 cylinder (11 mm inner diameter, 1 mm thick) embedded in the CsI crystal. The second geometry (square) uses a square BC-404 prism (11 mm inner side length, 1 mm thick) instead of the cylinder. In the third geometry (slab), the CsI crystal is cut in half, and the Xe cell is formed by two 50 mm $\times$ 50 mm $\times$ 1 mm BC-404 plates spaced at 1.4 mm distance.

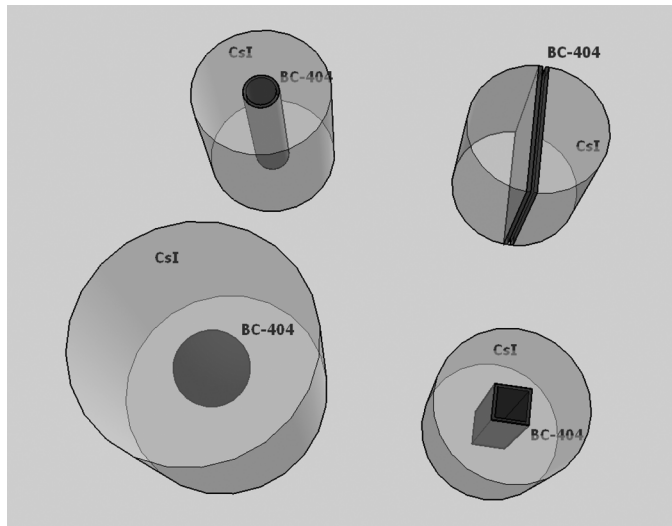

Fig. 1. Sketches of simulated phoswich geometries (clockwise from top left): PPW cylinder, PPW slab, PPW square, and PhosWatch.

TABLE II
Geometrical Properties

Geometry	CsI diameter x length (mm)	BC-404 inner distance	BC-404 thickness	Gas Volume
PhosWatch	76.2 x 76.2	11 mm (radius)	2 mm	5.6 cm^3
PPW Cylinder	50.8 x 50.8	11 mm (diameter)	1 mm	4.8 cm^3
PPW Square	50.8 x 50.8	10 mm	1 mm	5.1 cm^3
PPW Slab	50.8 x 50.8	1.4 mm	1 mm	3.6 cm^3

Geometrical properties of the simulated detectors. The length of the BC404 material is identical to that of the outer CsI material.

Table II defines the gas volume as well as inner and outer scintillator dimensions for each detector. The slab geometry was also modeled with a 2 mm Cu support frame acting as a vacuum seal around the Xe gas cell. The particles modeled in the simulations were 30, 80, 250, 662 keV photons and 129, 345, and 905 keV electrons. For each run $10^4 - 10^5$ particles were isotropically emitted from random locations within the gas volume. To simulate line broadening of the electron spectra and self-absorption of the photons, radioxenon was modeled as a uniformly distributed gas at standard temperature and pressure. The particles were tracked until they either exited the world volume or were absorbed in the detector materials. Optical photons emitted by the passage and/or absorption of these particles in the scintillating materials were tracked until "lost" at the polished dielectric-metal interfaces or absorbed (detected) at the photocathode. Fine tuning of the Geant resolution scale

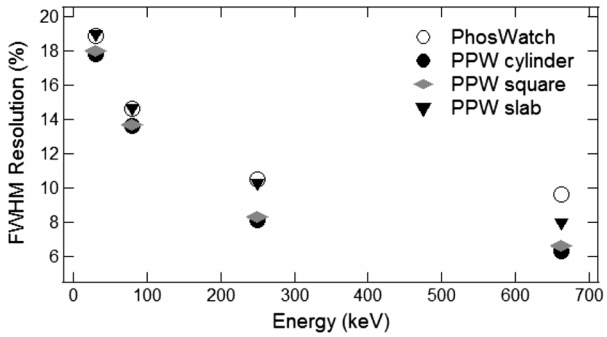

Fig. 2. Simulated energy resolutions at 30, 80, 250, and 662 keV.

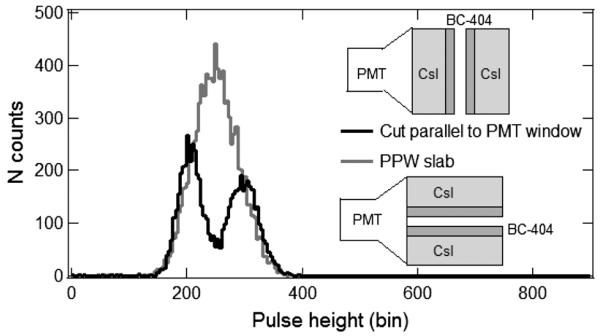

Fig. 3. The energy spectrum (30 keV) for the "bad" geometry shown in the upper sketch (black) and for the PPW slab geometry (lower sketch, gray).

and metal efficiency parameters was done in PhosWatch simulations based on the measured resolution at 662 keV obtained using a ^{137}Cs source [21]. These same parameters were then used in all subsequent simulations.

We define the energy resolution as the full width at half maximum (FWHM) from a Gaussian fit and the detection efficiency as the number of events in the full energy peak in each spectrum divided by the number of simulated events. Fig. 2 shows the simulated energy resolutions at 30, 80, 250, and 662 keV. Broadly speaking there is little difference in photon energy resolution between the various geometries. Errors in the FWHMs are smaller than the symbols and are on order of 0.1%

To verify that the simulation correctly describes "bad choices" in detector geometry, we also considered an extreme case: a PPW detector consisting of a stack of 50.8 mm diameter objects: CsI crystal, BC-404 cell, and CsI crystal (see inset in Fig. 3). Optical photons generated in the far CsI crystal must traverse the source volume to reach the PMT. Fig. 3 also shows the simulated energy spectrum showing two distinct peaks, which arise from gamma-rays interacting in the near and far CsI crystal (higher and lower energy peak, respectively). This geometry can, in principle, be improved by coupling a second PMT on the opposite face of the CsI crystal, though this approach runs contrary to the goal of this research to design a simple detector with a single PMT.

To describe the detector response with sufficient detail, we consider the following properties for photons. The results are listed in Table III.

TABLE III
DETECTION PROBABILITIES

Energy/ particle		Phos-Watch	Cy-linder	Square	Slab	Slab with frame
30 keV	CsI full	96.1	85.5	87.5	89.8	85.5
X -rays	BC404 part	6.2	3.6	3.9	7.6	
80 keV	CsI full	95.7	87.1	86.7	88.0	87.1
gammas	BC404 part	5.0	3.0	2.9	6.5	
250 keV	CsI full	89.5	67.3	67.3	70.6	73.7
gammas	BC404 part	3.6	2.3	2.2	5.1	
662 keV	CsI full	40.2	22.5	21.9	22.5	26.1
gammas	BC404 part	1.5	1.5	1.5	1.5	
129 keV	BC404 full	97.8	91.3	91.3	98.3	98.3
electrons	BC404 part	99.0	94.0	93.7	99.1	
	CsI part	0.21	0.24	0.3	0.2	
345 keV	BC404 full	97.4	88.4	88.7	96.4	96.9
electrons	BC404 part	98.8	93.4	93.6	99.0	
	CsI part	1.1	1.3	1.2	1.2	
905 keV	BC404 full	60.2	24.3	25.6	24.5	28.6
electrons	BC404 part	99.1	93.6	93.4	98.9	
	CsI part	54.6	77.7	75.7	69.2	

Probabilities for full and partial energy deposition, in percent. For the beta particles, only fixed energies were modeled, not beta energy distributions.

1. CsI full energy deposition, defined as the fraction of photons falling into the full energy peak of the energy spectrum, i.e. the gamma detection efficiency to be maximized,
2. BC-404 partial energy deposition, defined as the fraction of photons depositing significant energy (or all) in the BC-404, i.e. a value to be minimized and especially important for 30 keV X-rays.

Similarly for electrons:

1. CsI partial energy deposition, which is the fraction of electrons depositing significant energy in the CsI, i.e. the "punch through" for the BC404, which is to be minimized,
2. BC-404 full energy deposition, which is the fraction of electrons falling into the full energy peak in the energy spectrum, i.e. the detection efficiency for conversion electrons to be maximized,
3. BC-404 partial energy deposition, which is the fraction of electrons depositing significant energy in the BC404, i.e. the detection efficiency for beta particles (no fixed energy and therefore no peak), which is to be maximized.

There are two main effects that explain the difference in the photon detection efficiency between the PhosWatch and the PPW geometries seen in Table III. The first contribution is best seen at intermediate energies (e.g., 80 keV, where the photon path length is < 25.4 mm), where there is an $\sim 8\%$ difference in the probability for leaving the full energy in CsI. This difference is nearly entirely attributable to solid angle coverage lost from the open ends of the BC-404 cell. In the case of the 2" cylinder that solid angle loss is 8.6% - any gamma (or electron) hitting the open ends is lost. The second contribution becomes important when the path length of the photon exceeds the dimension of the detector. By 250 keV the escape probability emerges as the dominant contribution to the lowered efficiency. As with the photons, the electron efficiency for the PPW geometries suffers with respect to that of the PhosWatch, again due to solid angle coverage loss relating to the open ends of the BC-404 cell. At the highest energy of 905 keV the electron punches through the BC-404 and makes

TABLE IV
ESTIMATED BETA/GAMMA COINCIDENCE EFFICIENCIES

E (keV) photon	E (keV) electron	isotope	ε β/γ PW	ε β/γ cylinder	ε β/γ square	ε β/γ slab
30	129	^{131m}Xe	94%	78%	80%	88%
30	199	^{133m}Xe[1]	94%	78%	80%	88%
31	0-390	^{133}Xe[2]	95%	80%	82%	89%
80	0-345	^{133}Xe[2]	95%	81%	81%	87%
250	0-900	^{135}Xe[2]	89%	63%	63%	70%

[1] Assuming electron efficiency to be equal to 129 keV.
[2] Using electron efficiency from 345 (or 905) keV, any detected energy contributes

its way into the CsI volume. The lower value for the PhosWatch is due to its thicker BC-404 layer (2 mm versus 1 mm).

On the basis of photon response alone there is little difference in performance between the three PPW geometries. However, the electron response of the PPW slab is clearly better, presumably due to the large BC-404 surface area ($\sim 50\ \mathrm{cm}^2$) of the Xe cell. The probability of partial or full energy deposition would be expected to scale with surface area of the BC-404. Upon closer inspection a similar, but more subtle, effect is seen in the photon efficiencies.

Table IV lists the resulting beta/gamma detection efficiencies, i.e. the products of beta (or CE) and gamma efficiency for the energy combinations for the Xe isotopes of interest. The slab geometry has the highest detection efficiencies among the PPW geometries for all isotopes.

Overall, we therefore conclude the following: From all simulated PPW geometries, the slab geometry shows the highest detection efficiencies (especially for electrons) and lowest electron punch through, which is more important than the 1-2% smaller energy resolution in the other PPW geometries. (The slab energy resolution is still 0-2% smaller than the PhosWatch). The slab geometry is therefore our preferred choice for replacing the current PhosWatch geometry. All the PPW geometries have lower detection efficiencies for higher energy photons than the PhosWatch, but the overall loss is less than 10% for $^{133}\mathrm{Xe}$, $^{133\mathrm{m}}\mathrm{Xe}$, and $^{131\mathrm{m}}\mathrm{Xe}$, and about 20% for $^{135}\mathrm{Xe}$, resulting in a corresponding increase in MDC. This loss in efficiency is balanced by other advantages in the PPW geometries (cost, bulk, manufacturing, etc) and therefore deemed still acceptable.

B. Reducing the Memory Effect

Among the options to reduce the memory effect in BC-404 are coatings, protective layers, or alternate materials for the beta scintillator that do not absorb Xe. The former has been studied previously [8], [9], the latter two are considered here.

Alternative Materials: Several scintillators were considered as alternate materials, the main difficulty being finding a (manufacturable) thickness for which most electrons are absorbed and most X-rays pass unaffected. The most promising found were GS20 scintillator glass (though no manufacturer of custom shapes is available) and $\mathrm{YAlO_3:Ce}$ (YAP), previously tested for radioxenon detectors with inconclusive results [22].

As a first step, the continuous slowing down approximation (CSDA) ranges of electrons were determined for YAP, GS20 glass and BC-404. CSDA range constitutes a very close approximation to the average path length traveled by an electron as it slows down to rest [23]. Data were computed by the NIST eSTAR program [24] using "unique materials" close to the composition of YAP, GS20 glass and BC404. For electrons up to 345 keV (emitted by $^{133}\mathrm{Xe}$, $^{133\mathrm{m}}\mathrm{Xe}$, and $^{131\mathrm{m}}\mathrm{Xe}$,), the CSDA range is less or equal to 1.0 mm in BC-404, 0.5 mm in GS20, and 0.3 mm in YAP. For electrons up to 905 keV (emitted by $^{135}\mathrm{Xe}$), the CSDA range is less or equal to 3.9 mm in BC-404, 1.8 mm in GS20, and 1.0 mm in YAP.

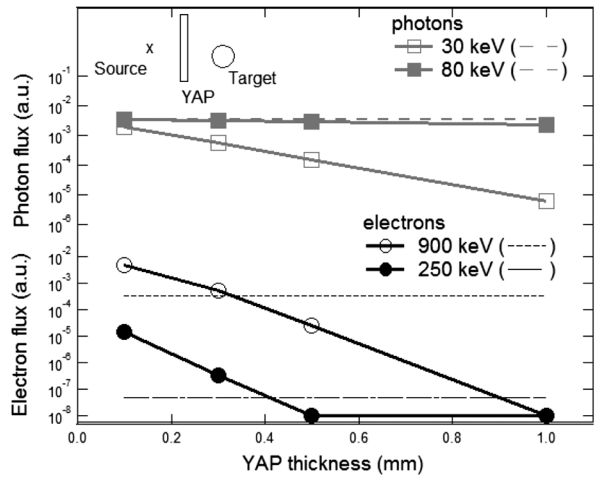

Fig. 4. Particle flux in MCNP simulation as a function of YAP thickness. Dashed lines indicate flux for 2 mm BC-404. To accommodate log representation, values of 0 are plotted at 10^{-8}.

However, at these thicknesses, the transmission of 30 keV X-ray also will be affected. The trade off between electron detection and photon absorption was thus studied as a second step using Monte Carlo N-Particle (MCNP) transport code simulations [25]. A simplified geometry was modeled with an isotropically emitting point photon/electron source placed 1 cm away from a large area sheet of YAP, GS20, or BC404 of various thicknesses. On the opposite side of the plate a target sphere of 5 mm radius was defined to measure the fluxes of simulated particles. The flux of particles detected in the target for the case of YAP is plotted in Fig. 4, indicating that for about 0.3-0.4 mm YAP or more, electrons are as effectively stopped as in 2 mm BC-404. This differs slightly from the CSDA results, which we attribute to the neglect of backscatter in the CSDA results and the differences in incident angles. However, for all thicknesses of YAP, fewer photons are detected than for 2 mm BC-404–at 0.3 mm the flux drops by $\sim 85\%$ for 30 keV and by $\sim 20\%$ for 80 keV. Overall, we compute that relative to 2 mm BC-404, the combined beta/gamma efficiency for $^{133}\mathrm{Xe}$ is about 43% with 0.5 mm YAP and 73% with 1 mm GS20. (For $^{131\mathrm{m}}\mathrm{Xe}$ and $^{133\mathrm{m}}\mathrm{Xe}$, which do not emit 80 keV gamma rays, the signal would be even further suppressed.) Overall, neither glass nor YAP is therefore desirable as a beta detector in the new phoswich detector.

Protective Layer: A thin metal foil, placed between the source and BC-404, also should prevent absorption of Xe into the BC-404 and suppress the memory effect. The foil should be metal to be a good Xe barrier, made from low Z material, and very thin; Titanium is one example of commercially available material. In this case there are two main concerns: a) low energy

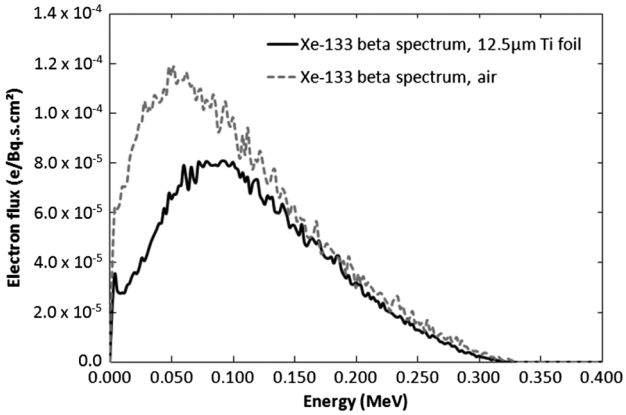

Fig. 5. Simulated ^{133}Xe beta spectra with and without Ti foil.

TABLE V
SENSITIVITY SUMMARY FOR PROTECTIVE LAYERS

	BC-404 + 12.5 μm Ti			BC-404 + 6 μm Ti		
	^{133}Xe	^{131m}Xe	^{135}Xe	^{133}Xe	^{131m}Xe	^{135}Xe
electron	0.55[1]	0.88[2]	0.89[1]	0.75[1]	1.00[2]	0.96[1]
photon	0.98[3]	0.96	1.00	0.99[3]	0.98	1.00
total	0.54	0.84	0.89	0.74	0.98	0.96

Simulated in MCNP for PhosWatch geometry.
[1] beta, [2] conversion electron, [3] 30 and 80 keV combined

electrons not passing through the foil and not being detected in the BC-404 and b) poor light collection due to additional reflection and absorption in the foil. Photon detection is of much less concern–a simple calculation using the NIST/XCOM program [26] shows very weak attenuation ($\sim 4\%$ and $< 1\%$) of 30 and 80 keV photons, respectively, by a 12.5 μm thin titanium foil.

Fig. 5 shows ^{133}Xe beta spectra from MCNP simulations (same geometry as above, but without YAP), through air (dashed) and a 12.5 μm thick titanium foil (solid) performed to quantify concern a). Comparing the areas under the curves we compute a 23% reduction for ^{133}Xe betas with Ti foil compared to air. ^{133}Xe CE emissions at 45 and 75 keV have a transmission factor of only 0.07. CE emissions from ^{131m}Xe and ^{133m}Xe are not significantly affected (transmission factors close to 1.00) due to their higher energy.

Loss of electrons and photons was estimated in more detail for a full MCNP model of the PhosWatch geometry with additional 12.5 or 6 μm Ti layers, respectively, Table V summarizes the results for most radioxenon isotopes of interest (^{133m}Xe is similar to ^{131m}Xe). All values are normalized to 2 mm thick BC404-only values, taken as the reference configuration with a sensitivity of 1. The electron energy threshold is set to 30 keV. For our purposes, the reduction of ^{133}Xe sensitivity to 74% with 6 μm Ti is still acceptable as a tradeoff for reducing the radioxenon memory effect, though a smaller reduction (with thinner or lighter material) is highly desirable.

The effect of a Ti foil on the light collection was studied again with the Geant model of the PPW slab geometry. Fig. 6 shows the optical photon spectra for 662 keV gammas from the slab detector with and without the Ti foil. Resolutions are 1-2% smaller with the foil (4.9% with vs. 6.3% without), indicating an improvement in light collection, presumably due to the reflectivity of the foil.

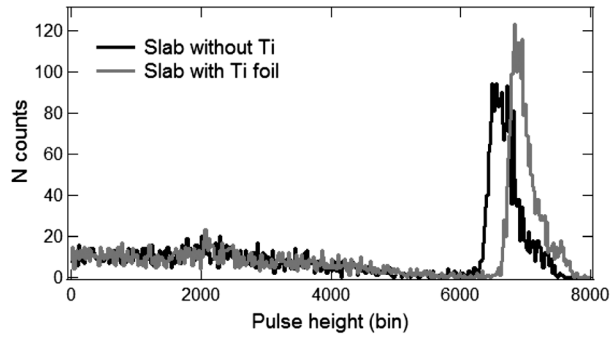

Fig. 6. Optical photon spectra for 662 keV gamma from the slab detector with the BC404 inner surface uncoated (black) and coated with Ti (gray).

C. Background

Since external radiation has a chance to interact with both scintillators and thus creates non-radioxenon coincidences, the detectors are usually shielded with layers of Cu and Pb. For a portable application, given the weight associated with the shielding, its thickness should be minimized without significantly affecting sensitivity. We therefore used the Geant model to estimate the minimum required lead shielding. A point source was defined outside the detector at a distance twice that of the CsI outer radius, with a plate of lead with varying thickness between source and detector. Two geometries were simulated: the PhosWatch and the PPW cylinder, both of which possess cylindrical symmetry and are therefore better suited for this simple background model with a point source. Events depositing energies within the region of interest (ROI), ($0 < \mathrm{E}_\gamma < 250$ keV) and ($0 < \mathrm{E}_\beta < 905$ keV), were recorded in a 2D energy plot. Results from interaction of 500 keV photons incident on the PPW cylinder detector with no Pb plate are shown in Fig. 7. The diagonal line is formed by those events where full energy is deposited in the detector but split between CsI and BC-404. Results from simulations of the two detector geometries at various energies and Pb plate thickness are listed in Table VI. At 100 keV, the photon energy is too low to generate events within the ROI as all are either absorbed in the Cu can or the CsI crystal. The maximum number of events that fall within the ROI is 729 out of 100,000 500 keV photons for the PPW cylinder with no shielding. The PhosWatch background count is also maximal under these same conditions. For energies above 500 keV, Compton scattering in the detector generally deposits more than 250 keV in the CsI, that is, outside of the ROI.

In Table VI, we assign each energy a relative weight derived from the observed background energy distribution in the PhosWatch. For example, in a background spectrum, roughly 8% of the counts fall in the range 1-2 MeV and so the simulated energy of 1.460 MeV carries a weight of 0.084. The weighted total of all simulated counts in the last rows thus represents the coincidence counts from the background energy distribution observed in the actual detector (very coarsely equating *detected* with *emitted* energy, which is sufficient precision for our purposes).

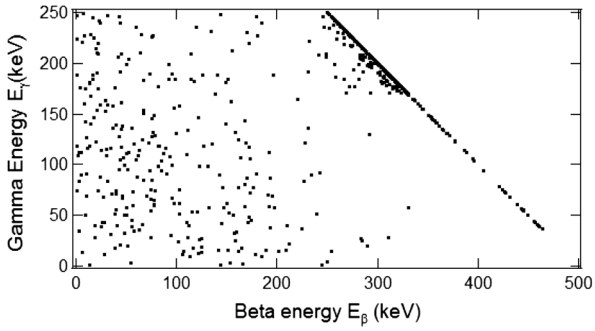

Fig. 7. 2D energy scatter plot for overall Xe region of interest from 100,000 500 keV external photons interacting in the PPW cylinder.

TABLE VI
COINCIDENCE COUNTS FROM EXTERNAL SOURCES WITH PB SHIELDING

	Energy (keV)	Rel. weight	0 mm	4 mm	10 mm	25.4 mm	50.8 mm
	100	0.594	0	0	0	0	0
PW	500	0.311	682	321	139	8	0
			±26	±18	±12	±3	
	1460	0.084	193	140	127	43	14
			±14	±12	±11	±7	±4
	2600	0.016	57	46	44	29	7
			±8	±7	±7	±5	±3
	10000	0.004	5	12	18	12	7
			±2	±3	±4	±3	±3
	weighted		229	112	55	6.6	1.3
	total		±15	±11	±7	±3	±1
	100	0.594	0	0	0	0	0
PPW	500	0.311	729	434	135	13	0
(cyl.)			±27	±21	±12	±4	
	1460	0.084	216	169	150	56	13
			±15	±13	±12	±7	±4
	2600	0.016	74	46	49	35	18
			±9	±7	±7	±6	±4
	10000	0.004	0	0	0	2	12
						±1	±3
	weighted		246	150	55	9.3	1.4
	total		±16	±12	±7	±3	±1

The MDC depends on the background BG according to [27]

$$\mathrm{MDC} \sim 2.71 + 4.65\,\mathrm{sqrt(BG)}. \tag{1}$$

Eq. (1) implies that as long as there are more than a few background counts in the total measurement, the MDC is proportional to the square root of the background. Previous tests [21] have shown the PhosWatch MDC to be between 0.2 and 0.5 mBq/m^3 with 50.8 mm lead and 12.7 mm Cu. An increase in background by a factor 4 - 25 would increase the MDC by a factor of 2 - 5 to the CTBT/IMS detection limit of 1 mBq/m^3. For the PPW to meet the limit, its weighted total should therefore be no more than 4–25 times the weighted total of the PhosWatch at 50.8 mm lead (1.3 counts), i.e. no more than 5.2–32.5 counts. According to Table VI, the PPW thus needs at least 25 mm lead shielding.

III. DETECTOR PERFORMANCE

From the above simulations, we concluded that the PPW slab geometry with 25 mm lead shielding and a less than 6 μm Ti foil would be the most promising design. As built, the detector deviated slightly from the design, due to accommodations made for manufacturing: A Cu frame is added between the BC-404 plates to form an air tight cell. The spacing of the BC-404 plates was adjusted so that the active volume is 6 cm^3 and instead of Ti foil a 2 μm Al coated mylar film (type B10HH, 32 nm Al) is used. Key simulations were repeated for the final design. The Cu frame modifies the detection probabilities by 2-3% (Table III), and adding the (lighter and much thinner) Al/mylar reduces the beta response by only 0.2% compared to 4-25% for adding 6 μm Ti.

A 9266KA PMT from ET Enterprises was coupled to the scintillator cell, and the complete detector assembly was placed in a OFHC cylindrical housing (2 mm wall thickness). A tube fitting brazed to the Cu frame is used to connect Xe gas tubing. The PMT was biased by a custom built power supply module (PSM), combining a Cockcroft-Walton style active HV base, a temperature sensor, and an LED pulser for gain stabilization. Detector, PMT and PSM are surrounded by 25 mm lead and packaged into a customized carrying case, total weight 32 kg. A single multi-signal cable connects the detector case to a PXI chassis with a XIA DGF Pixie-4 electronics module [28], which digitizes the detector signal, tags LED pulses for alternate processing, and applies the pulse shape analysis to detect coincidences and accumulate beta, gamma, and coincidence spectra [11]. A simplified software interface, Mobile OP, allows gain calibration and data acquisition, generating spectra files compatible with the IMS data standard.

After assembly, the detector (named PPW201) was tested with a variety of sources, solid $^{137}\mathrm{Cs}$, $^{133}\mathrm{Ba}$, $^{57}\mathrm{Co}$ and gas $^{222}\mathrm{Rn}$ and $^{133}\mathrm{Xe}$ placed externally and internally respectively. A selection of measured coincidence spectra is shown in Fig. 8. The spectra are equivalent to those from existing beta/gamma radioxenon detectors, such as SAUNA or ARSA. Subtle differences exist due to the detector geometry and the pulse shape analysis processing. For example, the "Compton line" from $^{137}\mathrm{Cs}$ does not have a sharp cutoff at $\sim$ 480 keV since the scattering process can take different paths. There is no clear CE "offset" of the lines formed by $\mathrm{CE} + \mathrm{beta} + \mathrm{X} - \mathrm{ray}$ decays ($^{133}\mathrm{Xe}$ at 30 keV and $^{222}\mathrm{Rn}$ at 80 keV) because the PPW has less than 4π coverage for electrons and so there is a chance for the fixed energy CE to escape and not be detected together with the beta. It is expected that these differences can be accommodated in existing spectrum analysis programs by slight adjustments of ROIs.

Energy resolutions from the measurements with solid sources are plotted in Fig. 9, comparing the results to two instances of the PhosWatch. As expected from the simulations, PPW201's resolution is equivalent to the PhosWatch. Variations of source location outside the detector showed that peak position and resolution vary by less than 2% and 6% of the total, respectively, which is within the precision of the measurement. Thus we conclude that this detector geometry does not significantly compromise the uniformity of the light collection.

To confirm the conclusion from simulations that 25 mm lead is sufficient shielding, the thickness of the lead was varied (without the carrying case) in a typical laboratory background. Count rates were recorded for all events, coincident events, and those coincidence events that would fall in a 30 keV $^{133}\mathrm{Xe}$ ROI, as plotted in Fig. 10. Measurements in the detector case

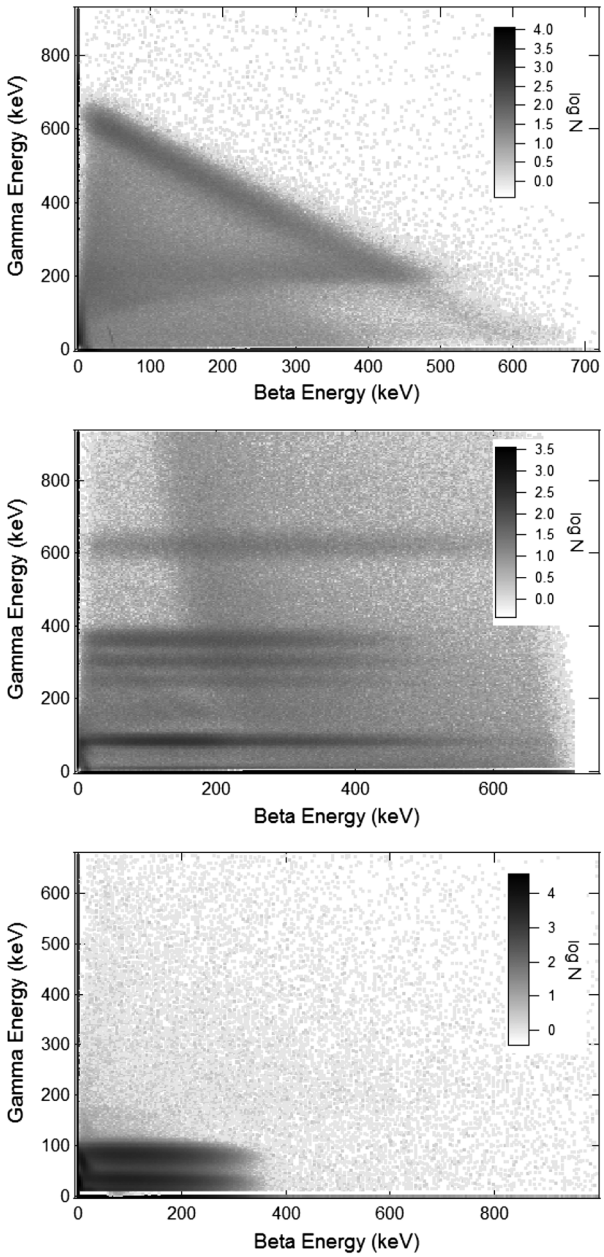

Fig. 8. 2D energy spectra from PPW201. Top: $^{137}\mathrm{Cs}$, middle: $^{222}\mathrm{Rn}$, bottom: $^{133}\mathrm{Xe}$. Compton scatter from external Cs source forms a diagonal line of constant energy. Beta/gamma coincidences from Rn and Xe form horizontal lines of fixed photon energy and a distribution of beta energies.

(25 mm lead) are marked as x. Extra points at 50.8 mm are from a PhosWatch, which has higher total background since it uses a larger CsI crystal.

Using (1), the change in MDC as a function of lead thickness t relative to 50.8 mm lead shielding can then be computed from $BC(t)$, the background counts in the ROI as

$$rel.MDC = \frac{2.71 + 4.65 * \sqrt{2BC(t)}}{2.71 + 4.65 * \sqrt{2BC(50.8)}}, \qquad (2)$$

plotted in the upper section of Fig. 10. The factor 2 assumes the 80 keV ROI has the same count rate as the 30 keV ROI,

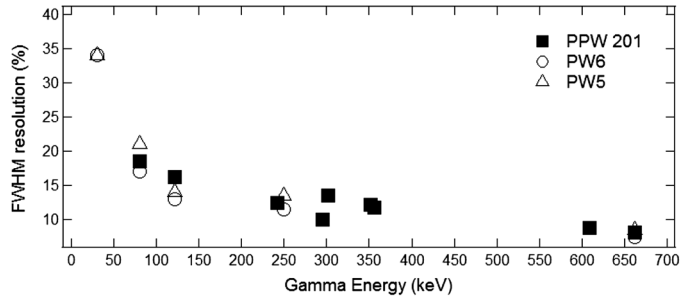

Fig. 9. Energy resolution as a function of energy for PPW201 and two PhosWatch detectors.

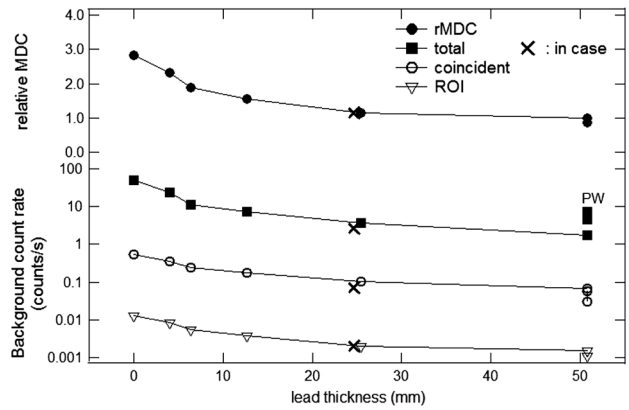

Fig. 10. PPW201 background counts and relative MDC as a function of shielding. The data points at "50.8 mm" stands for 50.8 mm lead and 12.7 mm Cu. Measurements in the detector case are marked with x.

the measurement time is assumed to be 24 h, and all collection parameters (volume air, processing time, etc) are assumed to be the same and cancel out. Overall, this is a coarse estimate of MDC changes due to background until calibrated radioxenon measurements can be performed. Compared to 50.8 mm lead shielding, the MDC is $\sim 15\%$ higher for 25 mm lead (or the detector case) and $\sim 55\%$ higher for 12.7 mm lead.

Since PPW201's ROI background is higher than the ROI background of the PhosWatch, the PhosWatch's MDC is $\sim 14\%$ lower at 50.8 mm lead shielding. We can use the measured MDC from a PhosWatch prototype, ~ 0.5 mBq/m^3 for $^{133}\mathrm{Xe}$ in one particular measurement, as a reference point (neglecting differences in efficiency, which may be significant), and estimate PPW201's MDC to be ~ 0.58 mBq/m^3 with 50.8 mm lead shielding and ~ 0.66 mBq/m^3 with 25 mm lead. These results thus indicate that 25 mm lead is indeed sufficient to reach an MDC below 1 mBq/m^3, as expected from the simulations.

In the background measurement following the Xe measurement, the net average coincidence count rate of PPW201 dropped to ~ 0.038 counts/s compared to ~ 10.6 counts/s during the Xe measurement. This corresponds to a memory effect of $0.4\% + / - 0.1\%$, compared to $7.9\% + / - 0.1\%$ for a PhosWatch (without mylar) operated in parallel. The mylar thus reduces the memory effect by more than one order of magnitude, to below the level of memory effect typical for any upstream gas processing system (roughly 1%).

IV. Conclusions

In summary, we modeled several new detector geometries with Monte Carlo simulations, showing that for most Xe isotopes the detection efficiency in a suitable 50.8 mm detector is only 6-8% lower than for an existing 76.2 mm detector. The simulations further indicate that energy resolutions are essentially unchanged and that 25 mm of lead shielding is sufficient to keep the MDC of the detector under 1 $\mathrm{mBq/m^3}$. The smaller size and thinner shielding reduce the overall weight of the detector built to 32 kg, compared to $\sim$ 400 kg for 4 detectors in a mobile SAUNA system [7]. Reduced complexity of the PPW detector design also lowered production costs by about a factor 3 compared to the PhosWatch.

A drawback for the new geometry is the coincidence detection efficiency for $^{135}\mathrm{Xe}$, which is $\sim 70\%$ compared to $\sim 90\%$ in existing detectors. Though this isotope is helpful to distinguish nuclear explosions from industrial sources, it is not expected to be present in OSI applications due to its short half life, and so we consider the lower efficiency an acceptable trade off for the reduced weight and cost.

Acknowledgment

The authors wish to thank Kai Vetter and Jeff Bickel at the University of California at Berkeley for providing the facilities and assistance with the Xe measurements.

References

[1] T. W. Bowyer, S. R. Biegalski, M. Cooper, P. W. Eslinger, D. Haas, J. C. Hayes, H. S. Miley, D. J. Strom, and V. Woods, "Elevated radioxenon detected remotely following the Fukushima nuclear accident," *J. Environ. Radioact.*, vol. 102, pp. 681–687, 2011.

[2] A. Ringbom, T. Larson, A. Axelsson, K. Elmgren, and C. Johansson, "SAUNA—a system for automatic sampling, processing, and analysis of radioactive xenon," *Nucl. Instrum. Methods Phys. Res. A*, vol. 508, pp. 542–553, 2003.

[3] J.-P. Fontaine, F. Pointurier, X. Blanchard, and T. Taffary, "Atmospheric xenon radioactive isotope monitoring," *J. Environ. Radioact.*, vol. 72, pp. 129–135, 2011.

[4] P. L. Reder, T. W. Bowyer, and R. W. Perkins, "Beta-gamma counting system for Xe fission products," *J. Radioanal. Nucl. Chem.*, vol. 235, pp. 89–94, 1998.

[5] E. Browne and R. Firestone, *Table of Radioactive Isotopes*. Hoboken, NJ, USA: Wiley, 1986.

[6] M. W. Cooper, J. I. McIntyre, T. W. Bowyer, A. J. Carman, J. C. Hayes, T. R. Heimbigner, C. W. Hubbard, L. Lidey, K. E. Litke, S. J. Morris, M. D. Ripplinger, R. Suarez, and R. Thompson, "Redesigned $\beta - \gamma$ radioxenon detector," *Nucl. Instrum. Methods Phys. Res. A*, vol. 579, pp. 426–430, 2007.

[7] M. Aldener, A. Axelsson, K. Elmgren, T. Fritioff, J. Kastlander, B. Lundberg, L. Mårtensson, A. Mörtsell, and A. Ringbom, "OSI noble gas equipment development," presented at the INGE Workshop , Vienna, Austria, Nov. 4–8, 2013.

[8] L. Bläckberg, A. Fay, I. Jõgi, S. Biegalski, M. Boman, K. Elmgren, T. Fritioff, A. Johansson, L. Mårtensson, F. Nielsen, A. Ringbom, M. Rooth, H. Sjöstrand, and M. Klintenberg, "Investigations of surface coatings to reduce memory effect in plastic scintillator detectors used for radioxenon detection," *Nucl. Instrum. Methods Phys. Res. A*, vol. 656, pp. 84–91, 2011.

[9] W. Warburton, W. Hennig, J. Bertrand, S. George, and S. Biegalski, "Alpha-Al2O3 diffusion barriers to eliminate the radioxenon memory effect in phoswich detectors," presented at the 34rd Monitoring Research Review, Albuquerque, NM, USA, Sep. 18–20, 2012, LA-UR-12-24325.

[10] J. H. Ely, C. E. Aalseth, and J. I. McIntyre, "Novel beta-gamma coincidence measurements using phoswich detectors," *J. Radioanal. Nucl. Chem.*, vol. 263, no. 1, pp. 245–250, 2005.

[11] W. Hennig, H. Tan, W. K. Warburton, and J. I. McIntyre, "Single channel beta-gamma coincidence detection of radioactive xenon using digital pulse shape analysis of phoswich detector signals," *IEEE Trans. Nucl. Sci. 53*, vol. 53, no. 2, pp. 620–624, Apr. 2006.

[12] A. T. Farsoni and D. M. Hamby, "A system for simultaneous beta and gamma spectroscopy," *Nucl. Instrum. Methods Phys. Res. A*, vol. 578, pp. 528–536.

[13] W. Hennig, C. E. Cox, S. J. Asztalos, H. Tan, P. J. Franz, P. M. Grudberg, W. K. Warburton, and A. Huber, "Study of silicon detectors for high resolution radioxenon measurements," *J. Radioanal. Nucl. Chem.*, vol. 296, pp. 675–681.

[14] G. Le Petit, A. Cagniant, M. Morelle, P. Gross, P. Achim, G. Douysset, T. Taffary, and C. Moulin, "Innovative concept for a major breakthrough in atmospheric radioactive xenon detection for nuclear explosion monitoring," *J. Radioanal. Nucl. Chem.*, vol. 298, pp. 1159–69, 2013.

[15] T. Schroettner, I. Schraick, T. Furch, and P. Kindl, "A high-resolution, multi-parameter $\beta - \gamma$ coincidence, $\mu - \gamma$ anticoincidence system for radioxenon measurement," *Nucl. Instrum. Methods Phys. Res. A*, vol. 621, pp. 478–488, 2010.

[16] V. Popov, "Beta-gamma coincidence spectrometer with Si PIN diodes," presented at the INGE Workshop, Vienna, Austria, Nov. 4–8, 2013.

[17] S. Agostinelli *et al.*, "Geant4-a simulation toolkit," *Nucl. Instrum. Methods Phys. Res. A*, vol. 506, no. 3, pp. 250–303, 2003, Geant4 Collaboration.

[18] J. Allison *et al.*, "Geant4 developments and applications," *IEEE Trans. Nucl. Sci.*, vol. 53, no. 1, pp. 270–278, Feb. 2006, Geant4 Collaboration.

[19] P. Mekarski, W. Zhang, K. Ungar, M. Bean, and E. Korpach, "Monte carlo simulation of a phoswatch detector using geant4 for xenon isotope beta–gamma coincidence spectrum profile and detection efficiency calculations," *Appl. Radiat. Isot.*, vol. 67, pp. 1957–1963, 2009.

[20] W. Hennig, H. Tan, W. K. Warburton, A. Fallu-Labruyere, J. I. McIntyre, and A. Gleyzer, "A phoswich well detector for radioxenon monitoring," *Nucl. Instrum. Methods Phys. Res. A*, vol. 579, no. 3, pp. 431–436, 2007.

[21] W. Hennig, W. K. Warburton, A. Fallu-Labruyere, K. Sabourov, M. W. Cooper, J. I. McIntyre, A. Gleyzer, M. Bean, E. P. Korpach, K. Ungar, W. Zhang, and P. Mekarski, "Development of a phoswich well detector for radioxenon monitoring," *J. Radioanal. Nucl. Chem.*, vol. 282, pp. 681–685, 2009.

[22] C. E. Seifert, J. I. McIntyre, K. C. Antolick, A. L. Carman, M. W. Cooper, J. C. Hayes, T. P. Heimbigner, C. W. Hubbard, K. E. Litke, M. D. Ripplinger, and R. Suarez, "Mitigation of memory effects in beta scintillation cells for radioactive gas detection," in *Proc. 27th Seismic Research Review: Ground-Based Nuclear Explosion Monitoring Technologies*, 2006, vol. 2, pp. 804–814, LA-UR-05-6507.

[23] eSTAR (stopping power and range tables for electrons) appendix, NIST [Online]. Available: http://physics.nist.gov/PhysRefData/Star/Text/appendix.html

[24] eSTAR (stopping power and range tables for electrons) program, NIST [Online]. Available: http://physics.nist.gov/PhysRefData/Star/Text/ESTAR.html

[25] [Online]. Available: https://mcnp.lanl.gov/

[26] XCOM program, NIST [Online]. Available: http://physics.nist.gov/PhysRefData/Xcom/html/xcom1.html://physics.nist.gov/PhysRefData/Xcom/html/xcom1.html

[27] L. A. Currie, "Limits for qualitative detection and quantitative determination," *Anal Chem.*, vol. 40, pp. 586–593, 1968.

[28] W. Hennig, Y. X. Chu, H. Tan, A. Fallu-Labruyere, W. K. Warburton, and R. Grzywacz, "The DGF Pixie-4 spectrometer–compact digital readout electronics for HPGe clover detectors," *Nucl. Instrum. Methods Phys. Res. B*, vol. 263, pp. 175–178, 2007.